Chinese Chemical Letters 34 (2023) 107957

Contents lists available at ScienceDirect

Chinese Chemical Letters

journal homepage: www.elsevier.com/locate/cclet

Advanced Pt hollow nanospheres/rubrene nanoleaves coupled with M-shaped DNA walker for ultrasensitive electrochemiluminescence bioassay

Yumeng Song[1], Xiuli Tao[1], Wenbin Liang, Xia Zhong*, Ruo Yuan, Ying Zhuo*

Key Laboratory of Luminescence Analysis and Molecular Sensing, Ministry of Education, College of Chemistry and Chemical Engineering, Southwest University, Chongqing 400715, China

ARTICLE INFO

Article history:
Received 6 July 2022
Revised 30 September 2022
Accepted 25 October 2022
Available online 28 October 2022

Keywords:
Platinum hollow nanospheres
Electrochemiluminescence aptasensor
M-shaped DNA walker
On-off-on switch
Carcinoembryonic antigen

ABSTRACT

Herein, an intense electrochemiluminescence (ECL) was achieved based on Pt hollow nanospheres/rubrene nanoleaves (Pt HNSs/Rub NLs) without the addition of any coreactant, which was employed for ultrasensitive detection of carcinoembryonic antigen (CEA) coupled with an M-shaped DNA walker (M-DNA walker) as signal switch. Specifically, in comparison with platinum nanoparticles (Pt NPs), Pt HNSs revealed excellent catalytic performance and pore confinement-enhanced ECL, which could significantly amplify ECL intensity of Rub NLs/dissolved O_2 (DO) binary system. Then, the tracks and M-DNA walker were confined on the Pt HNSs simultaneously to promote the reaction efficiency, whose M-structure boosted the interaction sites between walking strands and tracks and reduced the rigidity of their recognition. Once the CEA approached the sensing interface, the M-DNA walker was activated based on highly specific aptamer recognition to recover ECL intensity with the assistance of exonuclease III (Exo III). As proof of concept, the "on-off-on" switch aptasensor was constructed for CEA detection with a low detection limit of 0.20 fg/mL. The principle of the constructed ECL aptasensor also enables a universal platform for sensitive detection of other tumor markers.

The classic electrochemiluminescence (ECL) binary system based on coreactant pathway has drawn considerable focus in clinical diagnosis and laboratory research [1–4]. As an endogenous coreactant, dissolved O_2 (DO) could produce reactive oxygen species (ROS) in the electrochemical reaction to interact with emitters, which exhibits distinctive advantages of low toxicity and biocompatibility [5,6], while its weak redox activity restricts the application in trace substances detection. Recently, the metal nanomaterials [7] have been explored extensively due to obvious catalytic activity toward the electrochemical reduction of DO, such as palladium nanoparticles (Pd NPs) [8–10] and platinum nanoparticles (Pt NPs) [11,12]. Inspired by this, our group employed Pt NPs to efficiently enhance the ECL intensity of rubrene microrods/DO binary system in aqueous phases [13]. In comparison with solid nanomaterials, it was reported that hollow structures could prominently improve the catalytic performance of oxygen reduction reaction (ORR) [14–17] due to the pore confinement-induced enhancement [18] and the abundant surface active sites, which could generate more ROS to interact with the intermediates of emitters for significant improvement of the ECL intensity. Thus, Pt hollow nanospheres (Pt HNSs) were prepared in this work to achieve the outstanding ECL performance of rubrene nanoleaves (Rub NLs) based on the obvious catalytic effect of Pt HNSs on DO.

DNA walkers have widespread biological applications in biosensors construction for the detection of cancer-associated biomarkers [19–22], which hold merits including effective biometric recognition, quick target amplification, and timely signal conversion. Compared with the free DNA walkers, the DNA walkers with restricted tracks and strands [23] were demonstrated to increase the local concentration within the micro/nano space, resulting in efficient and continuous movement [24]. Yang *et al.* [21] described a highly efficient DNA walker that performed autonomous, stepwise movement along with high-density tracks on gold nanoparticles (Au NPs). More recently, DNA walkers have evolved from single-legged to multi-legged walking strands [25], which boosts the moving efficiency with the increase of interaction sites between walking strands and tracks. Sun and co-workers, for instance, proposed the linear dual-legged DNA walker amplification strategy to improve the walking speed and amplification efficiency for microRNA-21

* Corresponding authors.
E-mail addresses: zhonglyx@swu.edu.cn (X. Zhong), yingzhuo@swu.edu.cn (Y. Zhuo).
[1] These authors contributed equally to this work.

https://doi.org/10.1016/j.cclet.2022.107957
1001-8417/

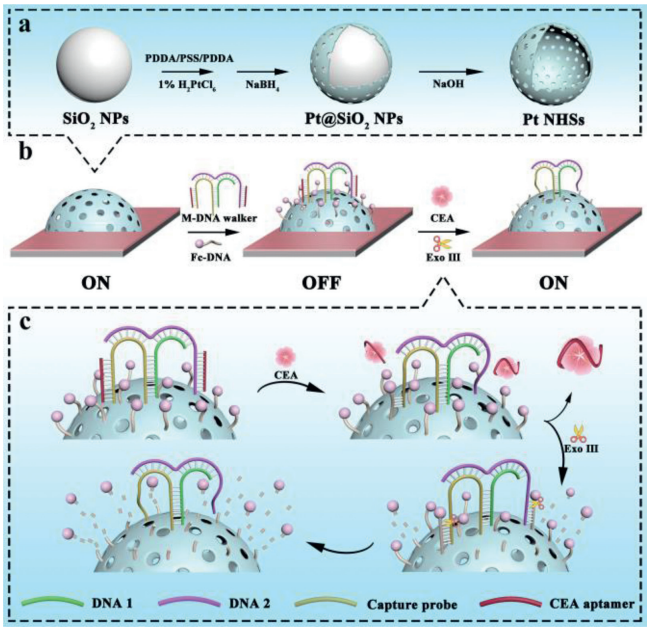

Scheme 1. Schematic illustration of the synthesis of Pt HNSs (a) and sensitive "on-off-on" ECL switch aptasensor based on the M-DNA walker for the detection of CEA (b and c).

detection [26]. Taking into account the matter of double strands rigidity in the linear dual-legged DNA walker, an M-shaped DNA walker (M-DNA walker) was designed in this work for mobility efficiency enhancement by reducing the rigidity of walking strands.

Herein, with the combination of ECL ternary system of Rub NLs/DO/Pt HNSs with an M-DNA walker, an ultrasensitive ECL aptasensor was constructed skillfully for CEA detection. Pt HNSs were obtained by etching away internal polyelectrolyte-modified colloidal silica (SiO_2) to obviously improve ECL reaction efficiency of Rub NLs (Scheme 1a). Impressively, Pt HNSs with the specific hollow porous nanostructure could offer more ROS generated by DO, which was ascribed to the pore confinement effect and the efficient catalytic property. The pore confinement effect not only concentrated abundant DO on the electrode surface but also effectively improved the electrochemical activity of redox-active species and shortened the proton and electron transport pathway for the reaction between Rub NLs and DO [27,28]. Simultaneously, Pt HNSs, as the matrix to anchor bioprobes, could directly attach DNA with amino-terminal groups through Pt-N coordination. Furthermore, in the presence of CEA, the enclosed M-DNA walkers confined on Pt HNSs were triggered by the highly specific binding of the aptamer, and one-step amplification of the signal was realized under the driving power of exonuclease III (Exo III) to achieve on-off-on signal switch (Schemes 1b and c). As proof of concept, the proposed ECL aptasensor achieved ultrasensitive detection of CEA with a wide linear (1 fg/mL ~ 1 ng/mL) and a low detection limit (0.20 fg/mL), which could also be extended to accurately quantify other tumor markers.

The scanning electron microscopy (SEM) pattern of Rub NLs was shown in Fig. 1a, which displayed leaf-like structures with a uniform size. The SEM image of Pt@SiO_2 NPs (Fig. 1b) confirmed that the surface became rough when Pt was generated on the surface of the polyelectrolyte-modified SiO_2 NPs (the SEM image of SiO_2 NPs was shown in Fig. S1 in Supporting information). Fig. 1c exhibited the SEM pattern of the Pt HNSs in revealing a regular spherical structure. Distinctly, from the transmission electron microscopy (TEM) images in Fig. 1d, it was evident that the internal space of Pt HNSs was empty compared to Pt@SiO_2 NPs (inset in Fig. 1d), indicating that the template of SiO_2 NPs had been removed. The N_2 adsorption–desorption technique was carried out to analyze the porosities of Pt HNSs, which further demonstrated the hollow nanostructure of Pt HNSs (Fig. S2 in Supporting information). X-ray photoelectron spectroscopy (XPS) of Pt HNSs was depicted in Fig. 1e, the existence of the metallic Pt was confirmed by the XPS doublet of Pt 4f (71.5 and 75.4 eV) (inset in Fig. 1e), proving the efficient generation of Pt HNSs. Meanwhile, the crystalline morphology of the Pt@SiO_2 NPs (curve I) and Pt HNSs (curve II) were revealed by typical X-ray diffraction (XRD) pattern (Fig. 1f). There were four diffraction peaks at 39.76°, 46.24°, 67.45° and 81.28°, respectively, which could point to (111), (200), (220) and (311) planar cubic (fcc) crystal Pt plane [JCPDS standard 01-1194 (Pt)], manifesting that the etching of SiO_2 NPs had no effect on the structure of Pt.

The UV–Vis absorption spectrum, fluorescence (FL) spectra and ECL 3D color map surface were monitored to investigate the optical properties of Rub NLs. As exhibited in Fig. 2a, the UV–vis absorption of Rub NLs presented three characteristic absorptions at 463 nm, 492 nm and 526 nm, respectively, which was consistent with reported work [13]. As depicted in the FL spectra (Fig. 2b), the maximum FL emission (Em) of Rub NLs was located at 559 nm with the excitation (Ex) of 463, 491 and 526 nm. It could be seen in the inset of Fig. 2b that the Rub NLs had bright orange fluorescence under the irradiation of UV light. Meanwhile, the ECL evolution process of the Pt HNSs/Rub NLs/GCE was recorded by the 3D color map surface (Fig. 2c), demonstrating the ECL maximum emission peak was located at 600 nm. To gain further insight into the electrochemical properties of Pt, the ECL-potential profiles of the Rub NLs/GCE, Pt NPs/Rub NLs/GCE and Pt HNSs/Rub NLs/GCE (Fig. 2d) were measured. Compared with Rub NLs/GCE, the noticeable increased ECL signal of Pt NPs/Rub NLs/GCE was observed, indicating the effective electrocatalytic activity of Pt NPs to enhance the ECL of Rub NLs/DO. Attentively, Pt HNSs, rather than Pt NPs, displayed a better performance of the signal enhancement effect on Rub NLs, which was attributed to the specific hollow porous nanostructure offering more ROS. Pt HNSs, on the one hand, possessed excellent electrocatalytic properties toward DO with abundant surface active sites. On the other hand, it provided a highly confined electrochemical reaction microenvironment to obtain intense ECL, namely pore confinement-enhanced ECL [18], which achieved efficient enrichment of DO and facilitated the reaction of Rub NLs and DO due to the reduction of the proton and electron transport pathway. Furthermore, the efficient electrocatalytic properties and the pore confinement effect of Pt HNSs could be confirmed by the cyclic voltammetry (CV) curves (Fig. S3 in Supporting information) as well.

We verified the feasibility of the aptasensor by native polyacrylamide gel electrophoresis (PAGE). Lane 1, 2, 3, 4 and 5 presented different single bands of DNA 1, DNA 2, CEA aptamer, capture probe and Fc-DNA in Fig. 3a, respectively, illustrating the rate of movement was related to the number of bases. When DNA 1, DNA 2, CEA aptamer and capture probe were hybridized by annealing, lane 6 revealed a bright band with a relatively slow movement, suggesting the successful formation of the M-DNA walker. When M-DNA walker, Fc-DNA, CEA and Exo III were added together in lane 7. It could be found two distinct bands corresponding to activated M-DNA walker and CEA aptamer, respectively. While the band of Fc-DNA was not observed, demonstrating that CEA aptamer bounded to the CEA to trigger the cleavage of Fc-DNA by M-DNA walker with the assistance of the Exo III. The ECL intensity-time response was then investigated to characterize the proposed modification process of aptasensor. As displayed in Fig. 3b, the bare GCE and Rub NLs/GCE exhibited a negligible ECL intensity (curve I, II) under the existence of DO with the scan range from −1 V to 1.2 V. After further modification of Pt HNSs on the Rub

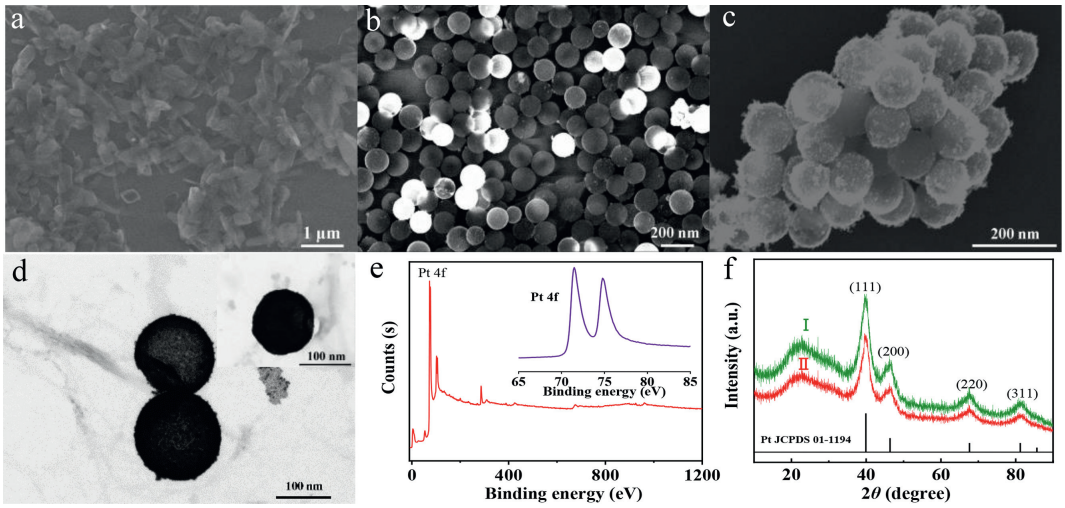

Fig. 1. SEM images of the Rub NLs (a), the Pt@SiO_2 NPs (b) and the Pt HNSs (c), TEM images of the Pt HNSs (d) and Pt@SiO_2 NPs (inset), XPS characterization for Pt HNSs (e), the XRD patterns (f) of Pt@SiO_2 (I) and Pt HNSs (II).

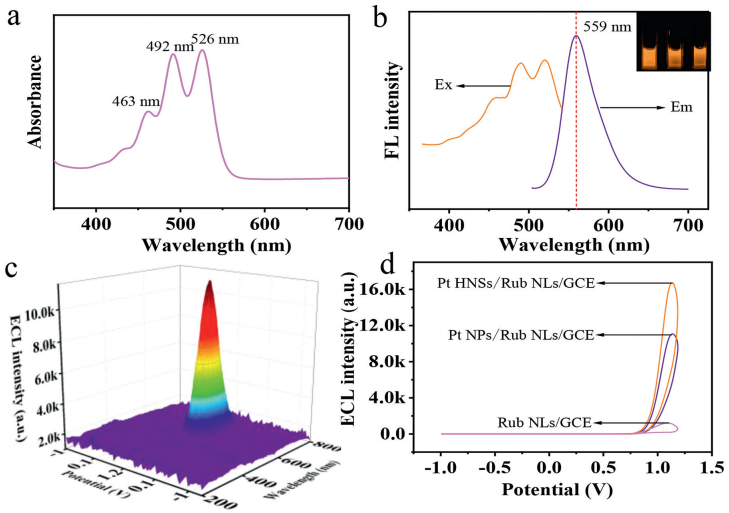

Fig. 2. (a) UV−vis absorption spectrum of Rub NLs. (b) Fluorescence excitation spectrum (Ex = 491 nm) and emission spectrum of Rub NLs (Em = 559 nm). The inset of b: photographs of Rub NLs under the radiation of UV light. (c) 3D color map surface of the Pt HNSs/Rub NLs/GCE. (d) ECL-potential profiles of Rub NLs/GCE, Pt NPs/Rub NLs/GCE and Pt HNSs/Rub NLs/GCE with the potential from −1 V to 1.2 V in 2 mL phosphate buffered saline (PBS, 0.1 mol/L, pH 7.4).

NLs/GCE (Pt HNSs/Rub NLs/GCE), a significant ECL emission peak (curve III) could be evidently observed. Owing to the obstruction of the M-DNA walker and the quench effect of Fc-DNA, the ECL intensity obviously declined (curve IV) when the M-DNA walker and Fc-DNA were incubated with the Pt HNSs/Rub NLs/GCE. Impressively, the ECL intensity significantly recovered again (curve V) while the reaction solution containing 10 ng CEA and 1 U/μL Exo III was incubated on the decorated electrode. Hence, in the presence of the CEA, M-DNA walker was activated to cleave the Fc-DNA with the help of the Exo III, which could act on double-stranded DNA and gradually cleave single nucleotides in the 3′→5′ direction. Furthermore, CV (Fig. S4 in Supporting information) was adopted to further verify the step-by-step fabrication of aptasensors.

The ECL intensity of the proposed aptasensor was positively correlated with CEA concentration (Fig. 4a) under the optimal conditions (Fig. S5 in Supporting information). As could be seen from Fig. 4b, a good linear relationship between the logarithm of the CEA concentration and the ECL signal was demonstrated by the calibration curve in the range from 1 fg/mL to 1 ng/mL with a low limit of detection (LOD) of 0.20 fg/mL. The regression equation for CEA was $I = 8433.55 + 1967.40$ lg$c$ with a correlation coefficient of 0.9990. Compared with other previous studies in Table S2 (Supporting information), our proposed method for CEA detection possessed excellent performance. The stability and selectivity were essential for aptasensor performance evaluation as well. As displayed in Fig. 4c, the CEA aptasensor exhibited consecutive signals with the relative standard deviation (RSD) of 1.27% in 10 cycles. Furthermore, possible interfering substances, such as alpha-1-fetoprotein (AFP, 10 ng/mL), C-peptide (C-P, 10 ng/mL) and β2-microglobulin (β2-MG, 10 ng/mL), were employed to verify the selectivity of aptasensor for CEA detection. It could be found that these interferences displayed no significant ECL signal recovery which was consistent with that of the blank in Fig. 4d. When the decorated electrodes were incubated with the CEA (1 ng/mL) and the mixture of AFP, C-P, β2-MG, and CEA, respectively, the noticeable ECL responses were recorded, indicating that the developed aptasensor had a favorable selectivity.

The potential of the proposed ECL aptasensors for clinical application was examined by adding a series of CEA with different concentrations in human serum. As shown in Table 1, the recoveries ranged from 97.2% to 103%, indicating that the developed ECL

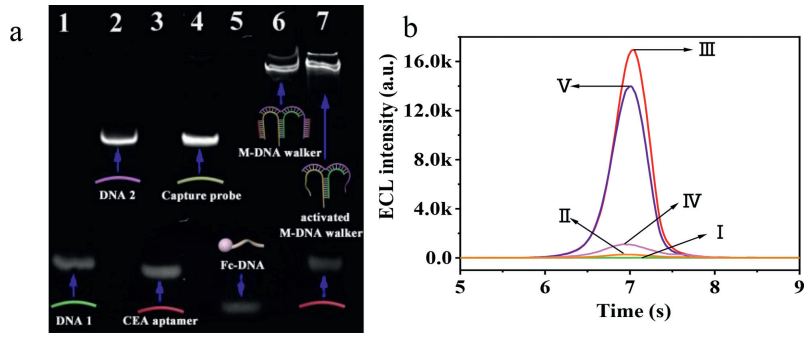

Fig. 3. (a) PAGE analysis of different samples: Lane 1, DNA 1; lane 2, DNA 2; lane 3, CEA aptamer; lane 4, Capture probe; lane 5, Fc-DNA; lane 6, M-DNA walker; lane 7, a mixture of M-DNA walker, Fc-DNA, CEA and Exo III. (b) ECL characterization of the modified electrodes implemented in 2 mL of 0.1 mol/L PBS (pH 7.4): (I) bare GCE; (II) Rub NLs/GCE; (III) Pt HNSs/Rub NLs/GCE; (IV) M-DNA walker/Fc-DNA/Pt HNSs/Rub NLs/GCE; (V) M-DNA walker/Fc-DNA/Pt HNSs/Rub NLs/GCE in the presence of Exo III and CEA.

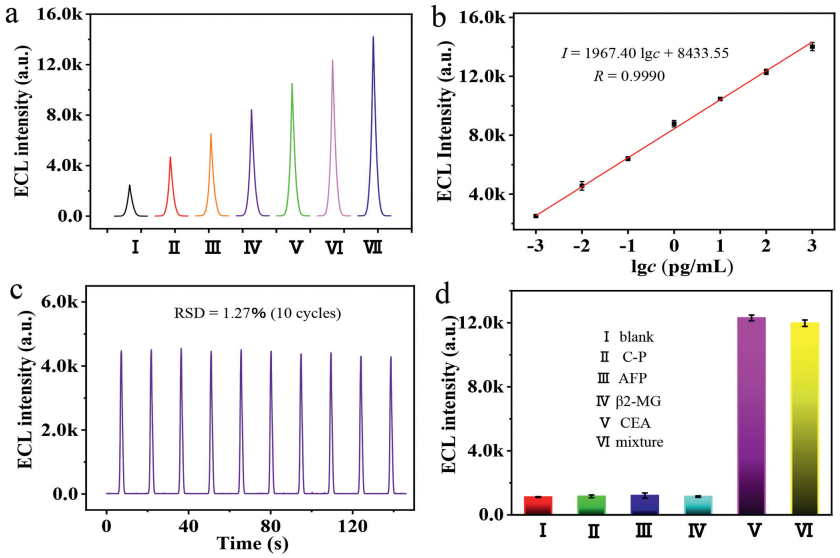

Fig. 4. (a, b) ECL responses of the aptasensors with different concentrations of CEA: (I) 1 fg/mL, (II) 10 fg/mL, (III) 100 fg/mL, (IV) 1 pg/mL, (V) 10 pg/mL, (VI) 100 pg/mL, and (VII) 1 ng/mL. (c) Stability of the proposed aptasensor under consecutive 10 cyclic potential scans. (d) Specificity of the CEA aptasensor: (I) blank, (II) 10 ng/mL C-P, (III) 10 ng/mL AFP, (IV) 10 ng/mL β2-MG, (V) 1 ng/mL CEA and (VI) a mixture of the samples above. Scanning potential range from −1 V to 1.2 V in 2 mL of 0.1 mol/L PBS (pH 7.4).

Table 1
The detection of CEA with the developed ECL aptasensors in human serum sample.

Sample number	Added (ng/mL)	Found (ng/mL, $n = 3$)	Recovery (%)
1	1.00	1.03	103
2	0.500	0.488	97.6
3	0.100	0.103	103
4	0.0500	0.0486	97.2

aptasensors were available for CEA detection in real biological samples.

In conclusion, an ultrasensitive ECL aptasensor with Rub NLs/DO/Pt HNSs as ECL ternary system was availably constructed for the CEA detection by coupling with M-DNA walker as signal switch. Notably, the specific hollow porous nanostructure of Pt HNSs could offer more ROS to enhance the ECL intensity of Rub NLs due to the pore confinement effect and efficient catalytic property towards DO. Furthermore, the enclosed M-DNA walkers confined on Pt HNSs were designed with low identification rigidity, which were triggered by CEA to achieve on-off-on signal switch. As proof of concept, the proposed aptasensor achieved ultrasensitive detection of CEA with excellent stability and selectivity, which presented a promising application prospect in the biochemical analysis of biomarkers. However, in terms of nanomaterials, some issues and challenges remain to be solved. For instance, the majority of the reported methods for the preparations of nanomaterials involve complex processes, which are unsuitable for industrial production and large-scale applications.

Declaration of competing interest

The authors declare no competing financial interest.

Acknowledgments

This work was financially supported by the National Natural Science Foundation (NNSF) of China (No. 22022408), the Chongqing Talents Personnel Support Program (No. NCQYC201905067) and the Fundamental Research Funds for the Central Universities (No. XDJK2019TJ002).

Supplementary materials

Supplementary material associated with this article can be found, in the online version, at doi:10.1016/j.cclet.2022.107957.

References

[1] F.A. Bushira, S.A. Kitte, Y. Wang, et al., Anal. Chem. 93 (2021) 15183–15191.
[2] L.F. Wang, J.J. Song, X.F. Wang, et al., Chin. Chem. Lett. 31 (2020) 2520–2524.

[3] Y.M. Nie, X.L. Tao, H.W. Zhang, Y.Q. Chai, R. Yuan, Anal. Chem. 93 (2021) 3445–3451.
[4] N. Hao, Y. Qiu, J.W. Lu, et al., Chin. Chem. Lett. 32 (2021) 2861–2864.
[5] J.L. Liu, R. Yang, Y.Q. Chai, R. Yuan, Anal. Chem. 93 (2021) 13334–13341.
[6] L. Wang, M.H. Jiang, Y.Q. Chai, R. Yuan, Y. Zhuo, Chem. Commun. 56 (2020) 9000–9003 (Camb).
[7] J.M. Xu, J. Ma, Y. Peng, et al., Chin. Chem. Lett. 34 (2023) 107527.
[8] H. Erikson, A. Sarapuu, N. Alexeyeva, et al., Electrochim. Acta 59 (2012) 329–335.
[9] W.Y. Si, Z. Yang, X.L. Hu, et al., J. Mater. Chem. A 9 (2021) 14507–14514.
[10] X. Liu, Q. Huang, J. Wang, et al., Chin. Chem. Lett. 32 (2021) 2086–2090.
[11] M.H. Shao, A. Peles, K. Shoemaker, Nano Lett. 11 (2011) 3714–3719.
[12] J.K. Tian, M.L. Zhao, Y.M. Song, et al., Anal. Chem. 93 (2021) 13928–13934.
[13] J.L. Liu, Z.L. Tang, Y. Zhuo, Y.Q. Chai, R. Yuan, Anal. Chem. 89 (2017) 9108–9115.
[14] K.D. Beard, D. Borrelli, A.M. Cramer, et al., ACS Nano 3 (2009) 2841–2853.
[15] H.P. Liang, H.M. Zhang, J.S. Hu, et al., Angew. Chem. Int. Ed. 43 (2004) 1540–1543.
[16] Y. Nie, J.H. Deng, W.T. Jin, et al., J. Alloy. Compd. 884 (2021) 161063.
[17] F. Xu, S.B. Cai, B.F. Lin, et al., Small 18 (2022) 2107387.
[18] Y.M. Lei, Y. Zhuo, M.L. Guo, Y.Q. Chai, R. Yuan, Anal. Chem. 92 (2020) 2839–2846.
[19] H.Y. Peng, X.F. Li, H.Q. Zhang, X.C. Le, Nat. Commun. 8 (2017) 14378.
[20] L. Song, Y. Zhuge, X.L. Zuo, M. Li, F. Wang, Adv. Sci. 9 (2022) 2200327.
[21] X.L. Yang, Y.N. Tang, S.D. Mason, J.B. Chen, F. Li, ACS Nano 10 (2016) 2324–2330.
[22] Y. Zhao, L. Tan, G.F. Jie, Sens. Actuators B: Chem. 333 (2021) 129586.
[23] H. Pang, X.W. Xu, W. Jiang, Sens. Actuators B: Chem. 314 (2020) 128053.
[24] N. Liao, M.C. Pan, L. Wang, et al., Anal. Chem. 93 (2021) 4051–4058.
[25] L.Y. Zhang, X.T. Liu, X.W. Xu, N. Zhang, W. Jiang, Sens. Actuators B: Chem. 327 (2021) 128942.
[26] M.F. Sun, J.L. Liu, Y.Q. Chai, et al., Anal. Chem. 91 (2019) 7765–7773.
[27] W.J. Zeng, K. Wang, W.B. Liang, et al., Chem. Sci. 11 (2020) 5410–5414.
[28] S. Fleischmann, M.A. Spencer, V. Augustyn, Chem. Mater. 32 (2020) 3325–3334.